RADAR IMAGES OF ASTEROID 1627 IVAR

S. J. OSTRO

Jet Propulsion Laboratory, California Institute of Technology, Pasadena, California 91109

D. B. CAMPBELL

National Astronomy and Ionosphere Center, Cornell University, Ithaca, New York 14853

A. A. HINE

National Astronomy and Ionosphere Center, Box 995, Arecibo, Puerto Rico 00613

I. I. SHAPIRO AND J. F. CHANDLER

Harvard–Smithsonian Center for Astrophysics, 60 Garden Street, Cambridge, Massachusetts 02138

C. L. WERNER AND K. D. ROSEMA

Jet Propulsion Laboratory, California Institute of Technology, Pasadena, California 91109

Received 28 November 1989

ABSTRACT

Radar echoes from the near-Earth asteroid 1627 Ivar, whose orbit crosses the Earth's, reveal it to be about twice as long as it is wide, with a maximum dimension no less than 7 km and probably within 20% of 12 km. The surface is fairly smooth at centimeter-to-meter scales but appears irregular and nonconvex at kilometer scales.

I. INTRODUCTION

Approximately 135 "near-Earth" asteroids have been discovered, all within the past century and most during the past decade. Whereas main-belt asteroids reside in relatively stable orbits and may have been formed close to their present locations, asteroids whose orbits can cross Earth's are relatively short lived and their formation locations conceivably might range from < 1 AU to > 10 000 AU. The known near-Earth asteroids have sizes that range from less than 100 m to several tens of kilometers; there are probably some 1000 objects with dimensions larger than 1 km (Shoemaker *et al.* 1979). The current near-Earth-asteroid population is thought to include extinct cometary nuclei as well as fragments of main-belt asteroids (Wetherill 1988; Wetherill and Chapman 1988). Here we report radar observations that provide novel constraints on the physical attributes of 1627 Ivar, one of the largest near-Earth asteroids and a readily accessible candidate for a spacecraft rendezvous (Lau and Hulkower 1987).

II. OBSERVATIONS

We observed Ivar with the Arecibo Observatory's 2380 MHz ($\lambda = 13$ cm) radar during 1985 July 5–10, when the object was 0.2 AU from Earth. The round-trip light time was ~3.3 min, so individual transmit–receive cycles ("runs") took about 6.6 min each. On five dates we did "cw" experiments, in which we transmitted a highly monochromatic, unmodulated, continuous wave and measured the distribution of echo power as a function of frequency. The resultant echo spectra can be thought of as one-dimensional images, or scans across Ivar's "disk" through a slit parallel to the asteroid's spin vector. We devoted July 9 to "ranging" runs, in which a time-coded waveform was transmitted and the distribution of echo power in time delay and frequency was measured, yielding two-dimensional images of the asteroid. Nominal radar system characteristics were: transmitter power, 440 kW; system temperature at zenith, 33 K; and one-way antenna gain at zenith, $10^{7.1}$. The transmission was always circularly polarized and echoes were received simultaneously in the same circular polarization as transmitted (the SC sense) and in the opposite (OC) sense.

Since the Arecibo telescope is located at 18° N latitude and cannot point more than 20° from the zenith, the hour-angle window for a target at Ivar's declination (8.2°–9.4°) during our observations was limited to 2.4 hr. Photoelectric observations of Ivar by Hahn *et al.* (1989) indicate that the asteroid's synodic spin period (*P*) during mid-July was 4.799 ± 0.001 hr, so we observed during the same half of a rotation cycle on each date. The most useful echoes cover somewhat less than 180° of rotation phase, because the telescope's sensitivity drops off sharply at high zenith angles. Figure 1 sketches the phase coverage provided by certain subsets of the data.

III. CONSTRAINTS ON PHYSICAL PROPERTIES FROM ECHO SPECTRA

To explore the dependence of Ivar's radar signature on rotation phase, we sorted the echo spectra into eight groups occupying contiguous, 22°-wide, rotation-phase intervals, and then formed weighted sums of all the spectra in each group (Fig. 2). We smoothed the sums from their original 1 Hz resolution to 4 Hz, to enhance the signal-to-noise ratio. During the observations, Ivar's radial motion relative to the radar introduced a continuously changing Doppler shift into the echoes, but we avoided the corresponding spectral smearing of the echoes by tuning the receiver to a prediction of the time dependence of the echo frequency based on an orbit determined from optical observations of Ivar. In Fig. 2, the frequency origin corresponds to the ephemeris's prediction for the frequency of hypothetical echoes from Ivar's center of mass (COM). The true COM frequency might be offset from the prediction, as discussed below.
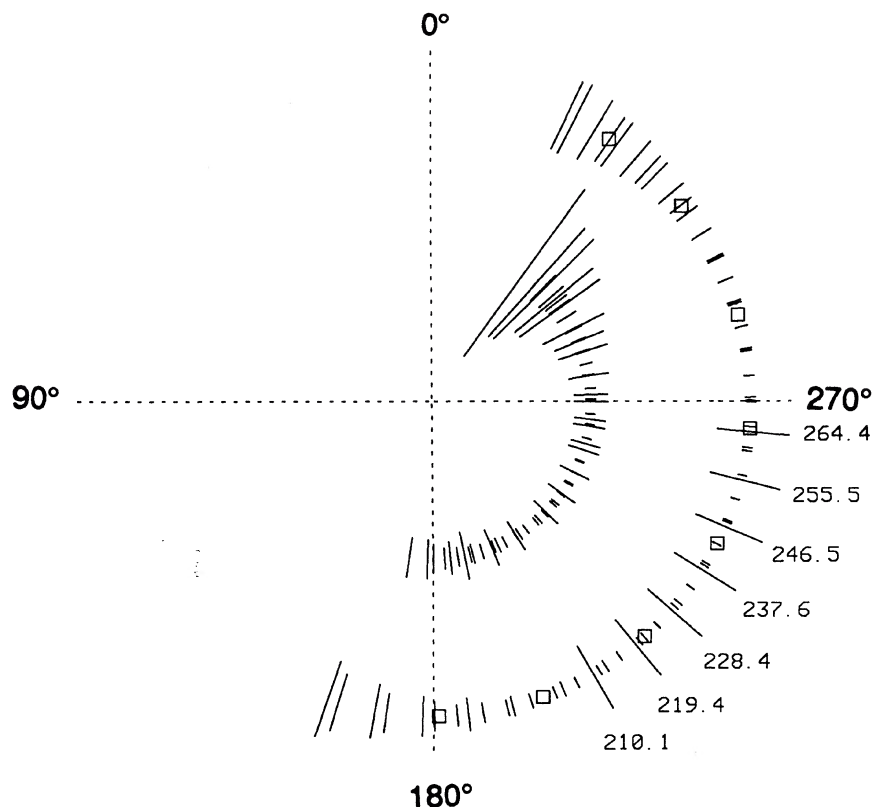
FIG. 1. Phase coverage of several subsets of the Ivar radar observations, based on an apparent rotation period of 4.799 h (Hahn *et al.* 1989). The (arbitrary) phase origin corresponds to reception of echo at 1985 July 9.20756 UTC. The seven labeled, short radial line segments indicate the phases, in degrees, of the delay-Doppler images obtained from observations taken on July 9. The rest of the radial lines indicate phases of cw (Doppler-only) runs and the lengths of these latter lines are proportional to the runs' relative noise levels. The outer ring shows phases of 57 runs from July 7, 8, and 10 that were used to make the eight spectra in Fig. 2; the eight squares indicate the weighted-mean phases of those spectra. The inner ring gives phases of the 68 spectra (the 47 lowest-noise spectra from the outer ring plus 21 spectra from July 5 and 6) that were used to estimate the convex hull of Ivar's pole-on silhouette, as discussed in the text. On July 5 and 6, problems with the transmitter's frequency synthesizer resulted in poorly calibrated echoes, precluding their use in cross-section determination. Using the cross-section estimate from the July 7, 8, and 10 spectra, we applied an *a posteriori* calibration to the July 5–6 spectra, which were then included in the hull estimations.

Each of the pairs of power spectra is labeled with our estimate of the OC radar cross section σ_{oc} and the circular polarization ratio μ_c, of SC to OC echo power. A weighted sum of all the dual-polarization spectra yields the values $\sigma_{oc} = 7.5 \pm 2.5$ km^2 and $\mu_c = 0.21 \pm 0.01$. The uncertainties correspond to estimated ~70% confidence intervals; the dominant contribution for σ_{oc} is system calibration errors, whereas for μ_c it is receiver noise fluctuations. The presence of detectable SC echo power indicates some near-surface roughness at centimeter-to-meter scales and/or some multiple scattering, but the dominance of the OC component indicates that most of Ivar's echo is due to single backscattering from surface elements that are smooth at those scales. On the other hand, the broad shapes of individual OC spectra suggest substantial structure at larger scales.

The most prominent attribute of the eight spectra in Fig. 2

is the variation in echo bandwidth B. As shown in Fig. 3, that quantity is related to the breadth D, measured normal to the radar line of sight, of the asteroid's pole-on silhouette (Ostro *et al.* 1988) by

$$B = (4\pi D \cos \delta)/\lambda P, \qquad (1)$$

where δ is the asteroid-centered declination of the radar. We have relatively low-noise spectra at the maximum-bandwidth phase, but the preceding minimum-bandwidth phase was observed only at large zenith angles, where competition from noise is extreme. Nevertheless, visual inspection of various subsets of our spectra establishes that the ratio D_{max}/D_{min} of the extreme breadths of Ivar's pole-on silhouette is approximately 2.0. Note from the σ_{oc} estimates in Fig. 2 that such extreme elongation would not be inferred from observed variations in radar brightness. Similarly, the
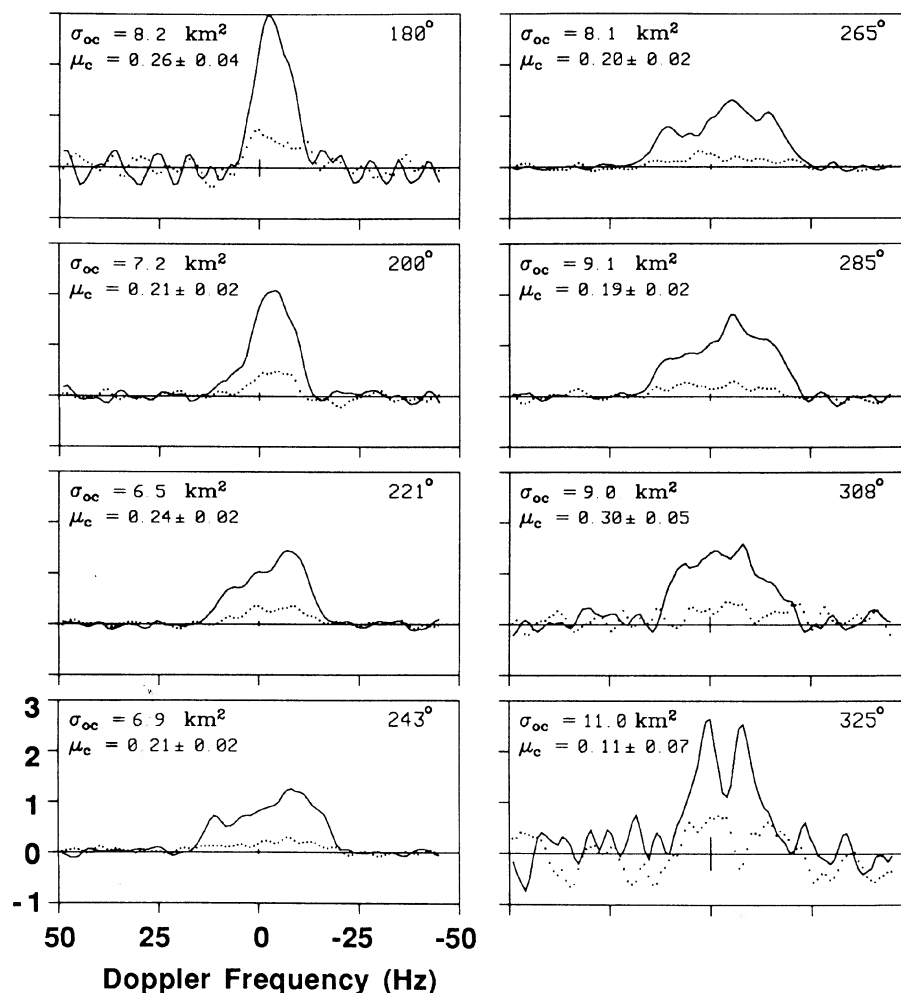
FIG. 2. Weighted sums of Ivar echo spectra. Weighted-mean rotation phases are indicated in the upper right corner of each panel. Echo power, in km^2 of radar cross section per 4 Hz frequency resolution cell, is plotted against Doppler frequency. The OC and SC echoes are shown as solid and dotted curves, respectively. On the abscissa, 0 Hz corresponds to hypothetical echoes from the asteroid's center of mass, according to our prediction ephemeris. The vertical bar at the origin of each plot shows ± 1 standard deviation of the noise. Estimates of radar cross section (σ_{oc}) and polarization ratio (μ_c) are given; for the estimates of σ_{oc}, the absolute (i.e., "calibration") uncertainty is $\sim 33\%$ and the relative uncertainty is $\sim 15\%$. Note that the fractional variation of μ_c with rotation phase does not seem very large, and that variations in σ_{oc} and echo bandwidth do not seem correlated with each other.

ratio of Ivar's optical brightness extrema during July 1985 was $\leqslant 1.5$ (Hahn *et al.* 1989). However, those authors' pole-direction estimates, derived from analyses of June–October 1985 lightcurves, correspond to values of δ between 50° and 70°, and brightness variations at such high sub-Earth latitudes would not be expected to disclose the object's full elongation.

Measurements of the "edge" frequencies of echo spectra as functions of the rotation phase of Ivar can be used to estimate the shape (and the size in units of km/cos δ) of the convex envelope, or "hull," of the target's pole-on silhouette as well as the offset f_0 of the COM frequency from the ephemeris prediction (Ostro *et al.* 1988; see Fig. 3). The hull is a pole-on projection of the asteroid with concavities "filled

in." As discussed by Ostro *et al.* (1990), the accuracy of a hull estimate depends on the signal-to-noise ratio, the frequency resolution, and the rotation-phase coverage and resolution of the spectra from which the edge frequencies are estimated. To assess the *a priori* reliability of hull estimates obtainable from the Ivar spectra, we conducted a lengthy series of simulations. Briefly, we generated spectra for a tri-axial ellipsoid model, contaminated the spectra with noise, and then estimated the model asteroid's hull. In the simulations, we chose the phase coverage, noise levels, and ellipsoid characteristics to ensure a reasonable degree of similarity between the model data and the Ivar data. Figure 4 superposes hull estimates (solid curves) for five noise realizations on the model's true, elliptical hull (dotted curve). The dis-
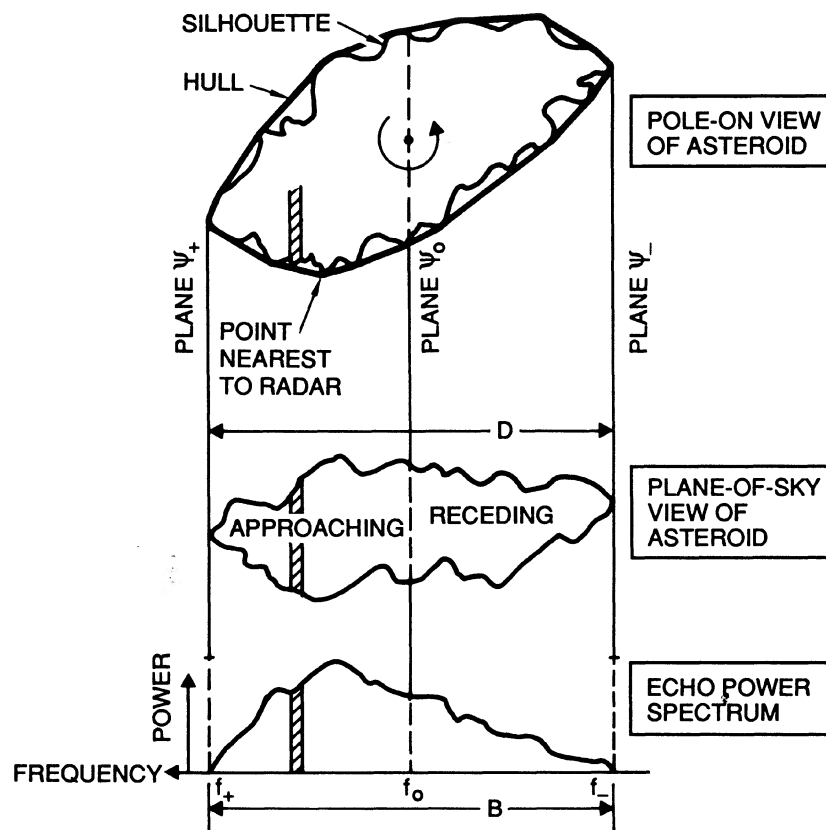
FIG. 3. Sketch of geometric relationships between an asteroid's shape and its echo power spectrum. The plane ψ_0, seen edge-on, contains the line of sight and the asteroid's spin vector. That plane is parallel to the planes Ψ_+ and Ψ_-. Equation (1) gives the relation between the echo bandwidth (B) and the breadth (D) of the asteroid's pole-on silhouette measured normal to the line of sight. Echo from any portion of the asteroid intersecting Ψ_0 has frequency f_0. The crosshatched strip of power in the spectrum corresponds to echoes from the crosshatched strip on the asteroid.

persion of the solid curves about the dotted curve provides a visual representation of the degree of uncertainty expected for the Ivar hull estimates discussed below. All estimations reported here use weighted-mean spectra with a phase resolution of 20° and the "raw" frequency resolution of 1.0 Hz; the simulations showed that different phase resolutions and/or coarser frequency resolutions do not improve the estimations' accuracy. Details of the (least-squares) hull-estimation procedure are described by Ostro *et al.* (1988, 1990).

The COM's location (in projection) within the hull and the odd harmonics in the Fourier-series expansion of the hull's shape are strong functions of f_0, which is treated as a free parameter in the hull estimation. However, our simulations showed that the sensitivity to f_0 is very poor because of the severely limited rotation-phase coverage of our Ivar spectra. (In the language of least squares, the minimum in chi square as a function of f_0 is poorly defined, where chi square is the sum of the squares of the differences between the measured edge frequencies and the "model" edge frequencies that correspond to the hull estimate.) Consequently, the odd harmonics in the shape of Ivar's hull and the

location of the COM inside the hull are also poorly constrained. Nevertheless, since the COM lies inside the hull, we know that the COM frequency f_0 lies within a band common to all the echo spectra. This requirement restricts admissible values for f_0 to the interval from about -12 Hz to about 8 Hz and also bounds the set of plausible hull estimates.

Figure 5 shows Ivar hull estimates derived from OC echo spectra (see Fig. 1 caption) for five values of f_0: -12, -7, -2, 3, and 8 Hz. The projection of the Ivar–Earth vector in the plane of the figure points toward the bottom of the page. Each hull is shown at three rotation phases whose relevance is discussed below. Note that the COM's location (the circled dot) is near the edge of the hull for f_0 equal to -12 or 8 Hz, whereas the COM is colocated with the hull's centroid (the square) for $f_0 = -2$ Hz.

The estimated shape of Ivar's hull is a strong function of f_0, but its size and elongation are not. The hull's maximum breadth (B_{max}) is estimated to be within 3 Hz of 43 Hz; the elongation (B_{max}/B_{min}), within 10% of 2.1; and the area of the hull, within 5% of 680 Hz^2, which is equivalent to 20.4 km^2/cos^2 δ. (The quoted bounds are estimated $\sim$70% con-
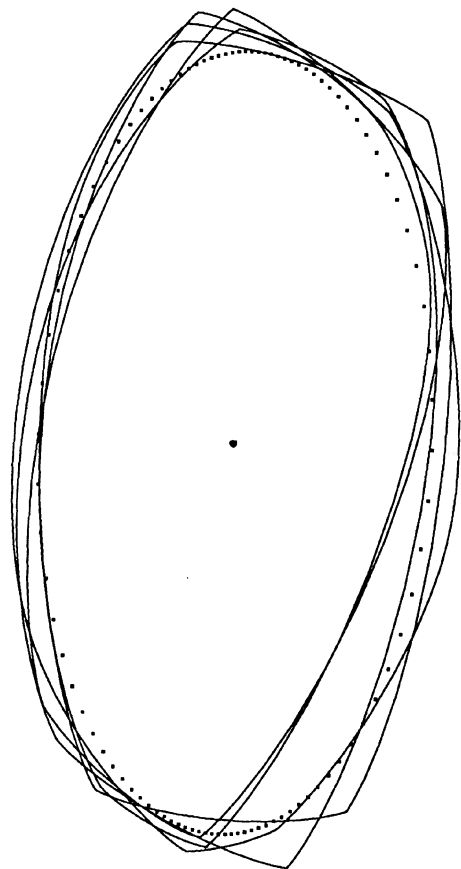
FIG. 4. Simulations designed to explore the accuracy of estimates of Ivar's hull. The dotted profile is the true hull of an ellipsoidal (convex) model asteroid and the solid curves are estimates derived from simulated echo spectra contaminated with noise. The five profiles correspond to five realizations of the noise-generating random process. The dispersion of the solid profiles about the dotted profile conveys the severity of statistical and systematic errors in Ivar hull estimates (Fig. 5) due to sources other than the uncertainty in the COM frequency offset f_0. See the text and Ostro *et al.* (1988, 1990).

fidence intervals.) The rotation phases presenting bandwidth extrema (B_{min}, B_{max}), and hence the pole-on silhouette's breadth extrema (D_{min}, D_{max}), are within a few degrees of (182°, 277°), again independent of f_0. Using Eq. (1) and our value for B_{max}, we obtain the constraint D_{max} = (7.4 ± 0.5) km/cos δ.

IV. DELAY-DOPPLER IMAGES

Independent information about Ivar's size and shape are provided by the ranging results from July 9, which consist of seven images (Fig. 6 [Plate 101]). Echo power is plotted as a function of time delay (range) and frequency in units of standard deviations, using the indicated gray scale. The time-delay resolution (8 μs) corresponds to a range resolution of 1.2 km. The frequency resolution is 3.8 Hz, corresponding to a distance resolution of 0.66 km/cos δ along the direction perpendicular to both the line of sight and Ivar's spin vector. These images, which sample phases from ~30° after the minimum-breadth orientation to ~10° before the maximum-breadth orientation (Fig. 1), show Ivar rotating

counterclockwise through ~54°. The asteroid extends over four to five range resolution "cells" (5–6 km) in the first three images, but is essentially unresolved in range in the seventh image.

If we had a nearly pole-on view of Ivar, the range distribution of echo power would not depend on rotation phase. Since our observations show dramatic contraction of the echo's range extent, we are skeptical that δ could have been as large as 70°. Certain quantitative results of our measurements must thus await better determination of Ivar's pole direction, but for purposes of illustration, let us adopt a subradar latitude of 50°. Under that assumption, the frequency resolution in Fig. 6 corresponds to a linear resolution of 1.0 km and our constraint on the pole-on silhouette's maximum breadth becomes D_{max} = 11.5 ± 0.8 km; we emphasize that the estimated standard error does not take into consideration the uncertainty in subradar latitude.

Suppose the portions of Ivar's surface that define its pole-on silhouette are close to the asteroid's equatorial plane, so that the silhouette's hull also represents Ivar's equatorial envelope. At the minimum-bandwidth orientation, the range extent of the hull would be D_{max} cos δ, or ~7.4 km for δ = 50°. The constraints on the hull's shape in Fig. 5 indicate that at the rotation phase of image 1, the range extent would be foreshortened to ~6.7 km, or ~5.5 range cells. Given the noise level in that image plus the fact that the most distant parts of the asteroid are unlikely to be illuminated, the four-range-cell extent of the echo seems in reasonable agreement with our estimate for D_{max} and the assumed value for δ. Image 7 is close to the maximum-bandwidth orientation, at which the hull's range extent is D_{min} cos δ, or roughly 3.5 km, or ~2.9 range cells. The echo is almost entirely contained within one range cell, but again we do not expect to see the object's full range extent. All factors considered, our dimensional constraints seem compatible with infrared-radiometric evidence that Ivar's "effective" mean diameter is within 10% of 9 km (Veeder *et al.* 1989).

Images 1 and 3 show a bimodal distribution of echo power in range. The last OC echo spectrum in Fig. 2, whose weighted-mean phase is roughly a quarter-cycle beyond the phase of image 3, also appears bifurcated. The statistical significance of the bifurcation in any one of these three echo power distributions is only several standard deviations, but taken together they argue for Ivar's radar brightness distribution being bimodal for certain orientations. A simple physical interpretation of this result is that the object's surface is nonconvex and very irregular at kilometer scales.

In each of these images, which range cell contains the center of mass? The answer to this question has implications for Ivar's mass distribution and for an accurate measurement of the absolute time delay for COM echoes, which can provide significant refinement in estimates of Ivar's orbital elements (e.g., Yeomans *et al.* 1987). The third image contains echoes in five range cells, numbered 835–839 (see Fig. 6 caption). During the asteroid's rotation, the delay contraction of the echo is fairly symmetric about delay cell 837. We suggest that this behavior is consistent with the COM's range-cell location being within two range cells or so of 837.5, and that it supports the hypothesis that the COM is not at the edge of Ivar's pole-on silhouette. Therefore, in the context of Fig. 5, we feel that the hull estimates for f_0 between + 3 Hz and − 7 Hz are probably more reliable than those for more extreme values of f_0. We have taken these considerations into account in assigning uncertainties to the radar astrometric

40 Hz

210 1
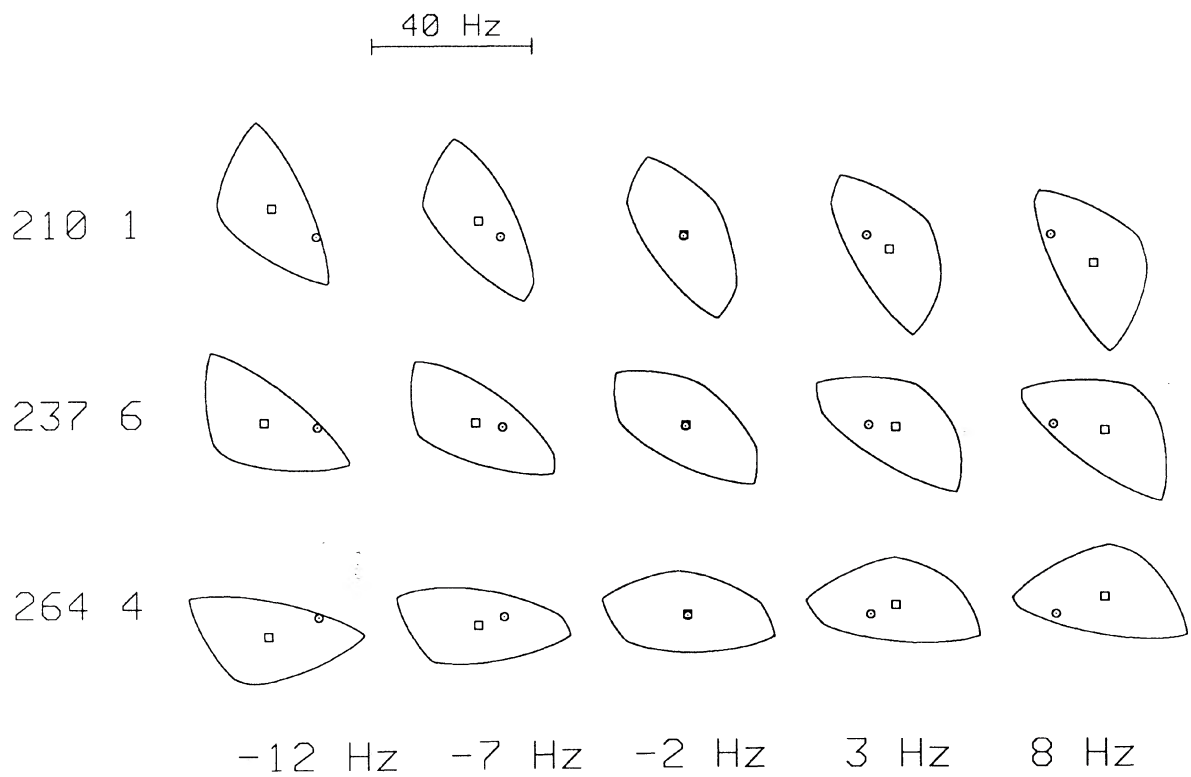
237 6

264 4

−12 Hz   −7 Hz   −2 Hz   3 Hz   8 Hz

FIG. 5. Estimates of the convex hull of Ivar's pole-on silhouette, shown for five values of the COM frequency offset f_0, as discussed in the text. The scale of the figures (in Hz) is indicated. The projection of the Ivar–Earth vector in the plane of the figure points toward the bottom of the page. For each value of f_0, the hull is shown at rotation phases of 210.1°, 237.6°, and 264.4°, corresponding to delay-Doppler images 1, 4, and 7 (Figs. 1 and 6). The circled dot locates the COM (and hence the spin vector) and the square locates the hull's centroid.

results in Table I. Table II gives estimates of Ivar's orbital elements, which we calculated using the results in Table I as well as all available optical astrometric observations of Ivar.

V. CONCLUSIONS

Despite the modest strength and limited phase coverage of the echoes, our experiment has provided unique information about Ivar's physical properties and the first two-dimensional image of an asteroid in the 10 km size range. Ivar's size and shape are reminiscent of Comet Halley's nucleus, but Ivar's optical and dynamical properties (Weissman *et al.* 1989; Hartmann *et al.* 1987; McFadden *et al.* 1984; Shoemaker *et al.* 1979) suggest formation in the main asteroid belt followed by a complex collisional history and ultimate delivery into an Earth-crossing orbit. Since collisions presumably have overwhelmed all other processes affecting small, inactive bodies in heliocentric orbits, Ivar and other small asteroids might constitute the largest irregularly shaped pieces of solid matter in nature. We expect ground-based radar to reveal these objects with increasing fidelity during the next few years. Improvements in the Arecibo radar telescope will permit dozens of Earth-approaching asteroids to be imaged at a signal-to-noise level about 20 times higher and a spatial resolution about 20 times finer than in the images presented here.

TABLE I. Radar astrometric results for asteroid 1627 Ivar. Measurements correspond to echoes from the (assumed) position of the asteroid's center of mass (COM); the standard deviations given include contributions from the uncertainty in estimating the location of the COM. Epochs are referred to the instant of reception at the Arecibo reference point, which is the center of curvature of the telescope's main reflector. The transmitter frequency is 2380 MHz.

Date (1985)	UTC hh:mm:ss	Doppler frequency (Hz)	Time delay (UTC μs)
July 8	08:00:00	20 560 ± 6	
July 9	08:09:00		202,574,571 ± 16

TABLE II. Osculating elliptic elements for 1627 Ivar for JED 2447800.5 referred to the mean ecliptic and equinox of B1950 as defined by the CfA's PEP740 planetary ephemeris. Angular elements are all in degrees and the semimajor axis is in AU. The uncertainties have been increased from the statistical standard deviations by a factor of about 3 to account for possible systematic errors.

Element	Estimate	Uncertainty (in last digit)
Semimajor axis a	1.86267259	6
Eccentricity e	0.3971428	3
Inclination i	8.44758	6
Long. asc. node Ω	132.6303	3
Arg. perihelion ω	167.3775	3
Mean anomaly l_0	236.7161	1

REFERENCES

Hahn, G., Magnusson, P., Harris, A. W., Young, J. W., Belkora, L. A., Fico, N. J., Lupishko, D. F., Shevchenko, V. G., Velichko, F. P., Burchi, R., Ciunci, G., Di Martino, M., and Debehogne, H. (1989). Icarus **78**, 363.

Hartmann, W. K., Tholen, D. J., and Cruikshank, D. P. (1987). Icarus **69**, 33.

Lau, C. O., and Hulkower, N. D. (1987). J. Guid. Control Dyn. **10**, 225.

McFadden, L. A., Gaffey, M. J., and McCord, T. B. (1984). Icarus **59**, 25.

Ostro, S. J., Connelly, R., and Belkora, L. (1988). Icarus **73**, 15.

Ostro, S. J., Rosema, K. D., and Jurgens, R. F. (1990). Icarus, **84**, 334.

Pettengill, G. H. (1970). In *Radar Handbook*, edited by M. I. Skolnik (McGraw–Hill, New York), Chap. 33.

Shoemaker, E. M., Williams, J. G., Helin, E. F., and Wolfe, R. F. (1979). In *Asteroids*, edited by T. Gehrels (University of Arizona, Tucson), p. 253.

Veeder, G. L., Hanner, M. S., Matson, D. L., Tedesco, E. F., Lebofsky, L. A., and Tokunaga, A. T. (1989). Astron. J. **97**, 1211.

Weissman, P. R., A'Hearn, M. F., McFadden, L. A., and Rickman, H. (1989). In *Asteroids II*, edited by R. Binzel, T. Gehrels, and M. S. Matthews (University of Arizona, Tucson), p. 880.

Wetherill, G. W. (1988). Icarus **76**, 1.

Wetherill, G. W., and Chapman, C. R. (1988). In *Meteorites and the Early Solar System*, edited by J. F. Kerridge and M. S. Matthews (University of Arizona, Tucson), p. 35.

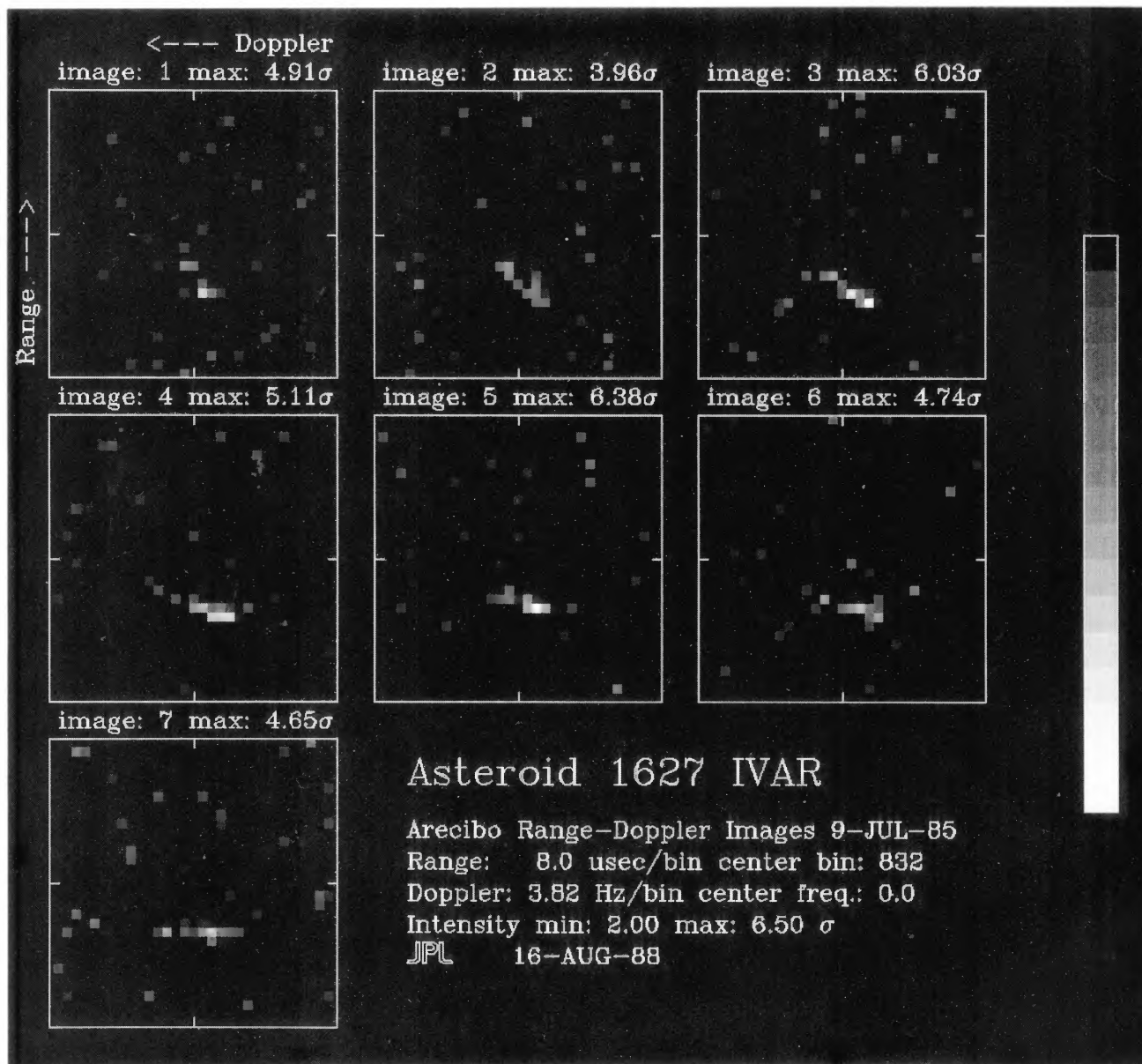Yeomans, D. K., Ostro, S. J., and Chodas, P. W. (1987). Astron. J. **94**, 189.

PLATE 101

FIG. 6. Radar images of Ivar obtained at rotation phases ~9° apart (Fig. 2). The integration time per run yields an intrinsic rotation-phase resolution of ~4°. Each image has been clipped from below at the two-standard-deviation (2.0σ) level to enhance the more prominent features of Ivar's echo. Echo power is plotted vs time delay (range) and Doppler frequency in units of standard deviations, using the indicated gray scale, which runs from 2.0σ to 6.5σ in equal, linear strips. The time-delay resolution (8 μs) corresponds to a range resolution of 1.2 km. The Doppler resolution is 3.8 Hz, corresponding to a distance resolution of 0.66 km/cos δ along the direction perpendicular to both the line of sight and Ivar's spin vector; the subradar latitude δ is not well known. The observations used a binary-phase-coded cw transmission with a 1023-element code, which permits resolution of echo power within 1023 independent range cells (e.g., Pettengill 1970). The 32 range cells from 827 to 858 are shown here; the relation between cell number and absolute time delay is known to within 1 μs and was used in the time-delay estimate in Table I. The 31 Doppler cells are centered on the frequency predicted by our ephemeris for echoes from the asteroid's center of mass, as in Fig. 2.

Ostro *et al.* (see page 2016)